P-Redox Mechanism at the Origin of the High Lithium Storage in NiP_2-Based Batteries

S. Boyanov,[†] J. Bernardi,[†] E. Bekaert,[‡] M. Ménétrier,[‡] M.-L. Doublet,*[,†] and L. Monconduit*[,†]

Institut Charles Gerhardt−CNRS−UMII−UMI−ENSCM, Université Montpellier II (Bât. 15), Place Eugène Bataillon, 34095 Montpellier, France, and CNRS, Université de Bordeaux, ICMCB, 87 Avenue Schweitzer, F 33608 Pessac, France

Received September 5, 2008. Revised Manuscript Received November 7, 2008

The Li reactivity of NiP_2 is investigated by means of electrochemical tests, in situ XRD, and ^{31}P NMR characterizations as well as first principles DFT calculations. A two-step insertion/conversion reaction is shown to transform the NiP_2 starting electrode into an intermediate Li_2NiP_2 single phase and then to convert into the Li_3P/Ni° nanocomposite. The ternary phase is fully characterized and is shown to be structurally very close to the starting NiP_2 regarding the Ni ions environment. This demonstrates that its formation results from a P-redox insertion mechanism associated with a very good reversibility. However, its nucleation upon delithiation from the fully converted Li_3P/Ni composite is shown to be kinetically limited (poor structural relationship) which strongly suggests that restricted lithiation is required for best cycleability of the NiP_2/Li cell.

1. Introduction

Rechargeable lithium ion batteries have progressively invaded the market, especially for portable electronic devices because of their high energy density. Since the commercialization of the $LiCoO_2$/C-based Li ion batteries by Sony, an important effort has been made to find alternative negative electrodes for the development of more powered and safe systems. Among the various candidates for negative electrode materials, the new conversion electrode materials offer numerous opportunities to reach impressive capacity gains. These electrodes can electrochemically react toward Li leading to sustainable reversible capacities as high as ~900 mA h g^{-1}, by the following conversion reaction: $M_xX_y + ny e^- + nyLi^+ \leftrightarrows xM^0 + yLi_nX$. Recently it was demonstrated that this Li reactivity mechanism was not specific to oxides but could also be found with sulfides, nitrides, fluorides, antimonides, and phosphides.[1−7] As compared to the classical insertion reactions, which are limited to $1e^-$ or even $0.5e^-$ per 3d metal atom ($LiCoO_2$), these new conversion reactions that can involve ne^- per 3d metal atom ($1 < n < 3$) were thought of as a new means to reach capacity gains. Efforts are under way to well-understand the redox mechanisms involved in such electrodes as well as their physical characteristics, with the idea to better control the cell and electrode properties.[8,9] Above all, it is of particular interest to understand the influence of the ligand (P) on such high capacities.

In this context, we recently reported the promising performances of NiP_2 as a negative electrode for Li-ion batteries.[10] Electrochemical measurements on the monoclinic NiP_2 starting material have shown a reversible exchange of 6 Li, leading to a gravimetric capacity of 900 mA h g^{-1}, which is stable after 20 cyles. From electrochemical, X-ray diffraction (XRD) and high-resolution electron microscopy (HRTEM) analyses, it was shown that NiP_2 first reacts with lithium through a two-phase insertion process ($NiP_2 + 2Li^+ + 2e^- \rightarrow$ "Li_2NiP_2") and then undergoes a conversion reaction which transforms the intermediate "Li_2NiP_2" electrode into a nanocomposite discharged electrode ("Li_2NiP_2" $+ 4Li^+ + 4e^- \rightarrow$ Ni° $+ 2Li_3P$). In this previous study, "Li_2NiP_2" was observed by in situ XRD techniques recorded during the first cycle. Since no Li_2NiP_2 phase is described in the literature so far, it is of great interest to characterize this electrode, as well as its role in the whole redox mechanism of the NiP_2 starting material. To identify the intermediate "Li_2NiP_2" electrode NiP_2/Li cell was discharged down to $x = 2$ and examined by TEM, in our previous work.[10] The high-resolution image showed that "Li_2NiP_2" was the result of stacking faults piling up between two

* Corresponding author. E-mail: Laure.monconduit@univ-montp2.fr (L.M.); Marie-Liesse.Doublet@univ-montp2.fr (M.-L.D.).
[†] Université Montpellier II.
[‡] Université de Bordeaux.

(1) Poizot, P.; Laruelle, S.; Grugeon, S.; Dupont, L.; Tarascon, J.-M. *Nature* **2000**, *407*, 496.
(2) Grugeon, S.; Laruelle, S.; Dupont, L.; Tarascon, J.-M. *Solid State Sci.* **2003**, *5*, 895.
(3) Débart, A.; Dupont, L.; Patrice, R.; Tarascon, J.-M. *Solid State Sci.* **2005**, *17*, 3627.
(4) Badway, F.; Cosandey, F.; Pereira, N.; Amatucci, G. G. *J. Electrochem. Soc.* **2003**, *150*, A1318.
(5) Villevieille, C.; Ionica-Bousquet, C. M.; Ducourant, B.; Jumas, J. C.; Monconduit, L. *; J. Power Sources* **2007**, *172*, 388.
(6) Boyanov, S.; Bernardi, J.; Gillot, F.; Dupont, L.; Womes, M.; Tarascon, J.-M.; Monconduit, L.; Doublet, M.-L. *Chem. Mater.* **2006**, *18*, 3531.
(7) Alcantara, R.; Tirado, J. L.; Jumas, J. C.; Monconduit, L.; Fourcade, J. O. *J. Power Sources* **2002**, *109*, 308.
(8) Breger, J.; Dupre, N.; Chupas, P. J.; Lee, P. L.; Proffen, Th.; Parise, J. B.; Grey, C. P. *J. Am. Chem. Soc.* **2005**, *127* (20), 7529.
(9) Cahill, L. S.; Yin, S.-C.; Samoson, A.; Heinmaa, I.; Nazar, L. F.; Goward, G. R. *Chem. Mater.* **2005**, *17* (26), 6560.
(10) Gillot, F.; Boyanov, S.; Dupont, L.; Doublet, M.-L.; Morcrette, M.; Monconduit, L.; Tarascon, J.-M. *Chem. Mater.* **2005**, *17* (25), 6327.

10.1021/cm802393z CCC: $40.75
Published on Web 12/19/2008

consecutive well crystallized regions, suggesting a single-phase electrode. From an electron diffraction study (SAED) a tetragonal cell was proposed as a rough estimate: $a = 5.5$ Å, $c = 4.2$ Å. For the fully discharged electrode, Ni nanoparticles were nicely observed by TEM, confirming the conversion reaction. Upon charge, XRD showed a continuous amorphization of the electrode. From HRTEM analysis it was proposed that upon charge the Ni°/Li_3P composite electrode reacts through a classical reverse conversion process leading back to NiP_2. This latter result must however be considered with caution because the HRTEM images could result from the presence of unreacted NiP_2 grains in the charged electrode, due to a partial conversion on first discharge.

Although the combined in situ X-rays and HRTEM data enabled us to identify the Li-reactivity mechanism of NiP_2, with namely an insertion process followed by a conversion process, both failed (i) in characterizing the intermediate "Li_2NiP_2" electrode and (ii) in identifying the nature of the recharged electrode. The main goal of this paper is to provide a structural assessment for the intermediate "Li_2NiP_2" and to determine the role of this electrode in the redox mechanism of NiP_2. To that concern we combine electrochemical studies on different restricted potential windows, in situ XRD, ^{31}P NMR characterizations, and first-principles Li/Ni/P_2 phase stability diagram computations. Merging these results leads to the full rationalization of the NiP_2 redox mechanism, showing that a P-redox mechanism is not only responsible for the high capacity of the electrode but also for its good cycleability.

2. Experimental Section

Electrochemical Tests. Swagelok-type cells were assembled in an argon filled glovebox and cycled using a VMP cycling/data recording system (Biologic Co, Claix, France) in a potential window between 2.5 and 2 and 0.02V vs Li^+/Li^0 and a cycling rate of C/10 (that is one lithium per formula unit in 10 h). These cells comprise a Li metal disk as the negative electrode, a Whatman GF/D borosilicate glass fiber sheet saturated with a 1 M $LiPF_6$ in ethylene carbonate (EC), dimethyl carbonate (DMC) (1:1 in weight) as the electrolyte, and a positive electrode made by mixing the starting transition metal phosphides powder with 15% (by weight) carbon black (SP). Usually, 10−12 mg of the mixed powders was placed on top of the Swagelok plunger.

In situ XRD electrochemical cells assembled similarly to our Swagelok cell but with a beryllium window as current collector on the X-ray side were placed on a Bruker D8 diffractometer (Cu Kα) equipped with a PSD detector, and connected to the VMP system. The cell was discharged at a *C*/10 rate and the X-ray powder patterns were collected for every 0.1 reacted Li.

NMR Spectroscopy. ^{31}P MAS NMR measurements were carried out with a Bruker Avance 300 spectrometer, using a standard Bruker 2.5 mm MAS probe, at a 30 kHz spinning speed. Materials recovered from positive electrodes were placed in the rotors in an Ar-filled glovebox. For ^{31}P NMR (121 MHz), a Hahn echo pulse sequence (with refocusing delay equal to one rotor period i.e. 33.3 μs) was used, the 90° pulse was 1.7 μs, and the recycle delay was varied depending on the sample. The reference is H_3PO_4 (85%), using a secondary solid-state reference $Al(PO_3)_3$ (−50.8 ppm). Decomposition and simulation of the spectra were achieved using the DMfit program.[11]

The samples were handled in glove-boxes and placed in 2.5 mm zirconia rotors that were proved to be sufficiently airtight for the time of the measurements (no change in the NMR signals). They were recovered from the electrochemical cells as follows: the first samples were washed to remove salt traces. Finally, because of the absence of overlapping between the spectra of phosphide and of $LiPF_6$, we decided to record NMR spectra of the samples as recovered from the cells.

Theoretical Tools and Models. First-principles density functional calculations were performed in the generalized gradient approximation (GGA) using the PBE functional[12] and the Projector Augmented Waves (PAW) pseudopotentials,[13] as implemented in the VASP code.[14] Various structural models were considered for the hypothetical Li_xNiP_2 phases, as already reported in refs 6 and 15. They correspond to fcc bulk of P atoms in which Ni and Li atoms lie either on the octahedral sites or on the tetrahedral sites, with ordered or disordered distributions. The crystal structure of the starting NiP_2 was also considered as an input structure for lithium insertion. These model structures were then fully relaxed for various lithium compositions and distributions. The convergence of the calculations was checked with respect to both the energy cutoff (600 eV) and the k-points grid (up to $9 \times 9 \times 9$ Monkhorst-Pac mesh) used for the Brillouin zone integration. Spin polarized calculations were considered to check the occurrence of Ni−Ni magnetic interactions in the phases of interest. As a comparative study to the conventional DFT calculations, the GGA+U formalism was also used[16,17] to check the influence of the Ni(3d) (on-site) electron correlation on the results of the calculations. This method allows for a better description of the electronic structure of strongly correlated systems, especially when the self-interaction error arising from a conventional DFT treatment becomes large. In practice, the noninteger occupations of the metallic 3d electronic levels are penalized by the introduction of two additional interaction terms, namely, the one-site Coulomb interaction term U, and the exchange interaction term J, by means of an effective parameter $U_{\text{eff}} = U - J$. Note, however, that although correlations effects are crucial to properly reproduce the electronic structure of transition metal oxides, they are expected to be minimized in the present case of transition metal phosphides, as a direct consequence of the much more covalent (more delocalized) character of the M−P bonds compared to the more ionic M−O bonds.

The Li−Ni−P_2 ($T = 0$ K) phase stability diagram was computed with respect to the conversion reaction, taken as the reference reaction. For that purpose, the formation energy (per formula unit) of each Li_xNiP_2 phase ($H(Li_xNiP_2)$; $0.25 \le x \le 5$) is compared to the reference energy of the conversion reaction (proportional mixture of the starting NiP_2 and the discharge $2Li_3P$ + Ni° electrodes) using the simple expression

$$\Delta H(x) = H(Li_xNiP_2) - \left\{\left(1 - \frac{x}{6}\right)H(NiP_2) + \frac{x}{3}H(Li_3P) + \frac{x}{6}H(Ni^\circ)\right\} \quad (1)$$

The simulated XRD patterns and the density of states (DOS) of the most relevant phases were then computed in order to correlate their crystal and electronic structures to the in situ XRD and the

(11) Massiot, D.; Fayon, F.; Capron, M.; King, I.; Le Calvé, S.; Alonso, B.; Durand, J.-O.; Bujoli, B.; Gan, Z.; Hoatson, G. *Magn. Reson. Chem.* **2002**, *40*, 70.
(12) Perdew, J. P.; Burke, S.; Ernzerhof, M. *Phys. Rev. Lett.* **1996**, *77*, 3865.
(13) Perdew, J. P.; Burke, S.; Ernzerhof, M. *Phys. Rev. Lett.* **1996**, *77*, 3865.
(14) Kresse, G.; Hafner, J. *Phys. Rev. B* **1993**, *47*, 558. (a) Kresse, G.; Furthmuller, J. *Comput. Mater. Sci.* **1996**, *6*, 15.

^{31}P NMR experimental signatures obtained for the electrodes achieved at various steps of charge and discharge.

3. Results

The monoclinic NiP_2 phase was synthesized at high temperature (900 °C/5 days) as previously reported by placing stoichiometric amounts of nickel metal and red phosphorus powders in a sealed evacuated silica ampule.[10,18] As-obtained powder is made of shapeless particles having an average size ranging from 5 to 50 μm. NiP_2 cristallizes in the $C2_1/c$ space group with lattice parameters (a = 6.38 Å, b = 5.62 Å, c = 6.08 Å, β =126.22°). Within the NiP_2 monoclinic unit cell, Ni is simply coordinated to 4 P atoms in a square-planar environment suggesting a Ni^{+II} (d^8) electronic configuration. For the Li_3P synthesis, ball-milling experiments (denoted hereafter BM) were performed using a Retsch 200 mixer mill that generates normal mechanical strain.[19] The grinding vial loading and sealing was done in an argon dry box. Required amounts of Li and red P precursor powders were placed into a stainless steel container together with steel balls in a weighted ratio of steel ball to powder of 24:1. After 18 h of grinding, the vial was opened in the dry box, and the powder was characterized for their phase purity by X-ray diffraction.[19]

3.1. Electrochemical Properties. To characterize the "Li_2NiP_2" intermediate electrode, NiP_2/Li cells were assembled and tested for their electrochemical behavior at a C/10 rate on the limited potential windows [0, 2 V], [0.25, 2.5 V], [0.31, 2.5 V], and [0.44, 2.5 V]. For the first discharge, the low-potential limits correspond to the lithium contents x = 5.9, x = 3.6, x = 2.2, and x = 1.5, respectively (Figure 1a−d)). To better identify the electrochemical processes, we also plotted the derivatives of each voltage/composition trace (Figure 1a−d). Depending on the potential range, one or two incremental peaks are observed on the first discharge derivative curve (dashed gray lines). The first peak at 0.5 V (labeled 1) was previously assigned to the NiP_2 → "Li_2NiP_2" transformation and the second at 0.3 V (labeled 2) to the "Li_2NiP_2" → Ni°/Li_3P conversion reaction.[10] The application of these potential cut-offs obviously change the nature of the electrode obtained in discharge, prior to the further oxidation procedure: if one assumes the two successive processes to be classical multiphased reactions, the discharged electrodes correspond to the nanocomposite Ni°/Li_3P at 0 V, a mixture of "Li_2NiP_2" and Ni°/Li_3P at 0.25 V, the intermediate "Li_2NiP_2" electrode at 0.31 V, and a mixture of NiP_2 and "Li_2NiP_2" at 0.44 V.

On the [0, 2 V] Potential Window. On the full [0, 2 V] potential window (Figure 1a), a broad oxidation peak denoted A is observed at 1.13V (with a shoulder S) which was previously ascribed to the reconstruction reaction Ni°/Li_3P → NiP_2. On discharge, a very broad peak B (0.4 V wide) is centered at 0.7 V. A sharp peak is then observed at 0.62 V that slightly overlaps peak B, namely, peak C. These two peaks were previously associated with the two-step Ni°/Li_3P electrode formation from NiP_2.[8]

On the [0.25, 2.5 V] Potential Window. On the [0.25, 2.5V] potential window, we simultaneously observe a decrease of the area under the oxidation peak A and of the reduction peaks B and C (Figure 1b). Correlatively, a new pair of peaks appears denoted D on charge and E on discharge. In this potential range the "Li_2NiP_2"/Ni°/Li_3P mixed electrode is expected to be formed at the end of the first discharge. This new D/E process is then directly linked to the reaction of "Li_2NiP_2" on charge and discharge, in the composition range $0 \leq x \leq 2$.

On the [0.31, 2.5 V] and [0.44, 2.5 V] Potential Windows. On the [0.31, 2.5 V] and [0.44, 2.5 V] restricted windows (panels c and d in Figure 1, respectively), the reduction peaks B and C and the oxidation peak A are nearly absent, while the E/D peaks are predominant. Note that S is still present. In both cases, the electrode at the end of the

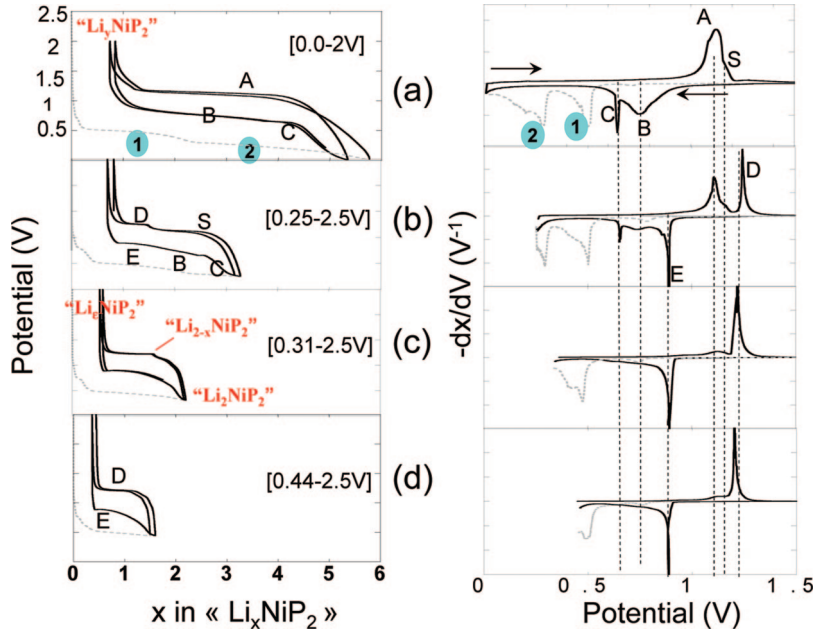

Figure 1. Voltage−composition curves (left) and their associated −dx/dV derivative plots (right) for NiP_2 /Li cells cycled at a C/10 rate between (a) 2.0 and 0 V, (b) 2.5 and 0.25 V, (c) 2.5 and 0.31 V, and (d) 2.5 and 0.44 V.

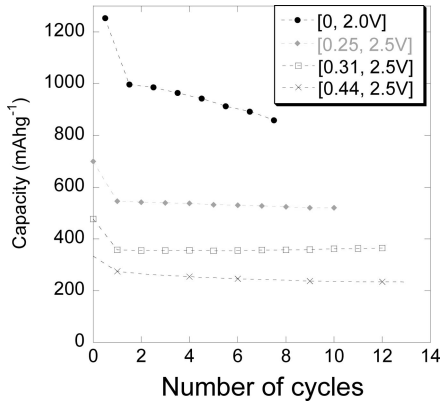

Figure 2. Cycleability of NiP_2 /Li cells cycled at a *C*/10 rate between (a) 2.0 and 0 V, (b) 2.5 and 0.25 V, (c) 2.5 and 0.31 V, and (d) 2.5 and 0.44 V up to 12 cycles.

first discharge is expected to be mainly "Li_2NiP_2". This confirms that D is associated with the lithium extraction from "Li_2NiP_2" up to "$Li_\varepsilon NiP_2$" and E to the further lithiation of the "$Li_\varepsilon NiP_2$" electrode formed in charge at the end of D. These two peaks are very sharp, as typically observed for two-phase processes for which the phase transition is kinetically limited by the front phase migration.[20] This two-phase reversible D/E process is confirmed by the voltage plateau on the galvanostatic curves of panels c and d in Figure 1.

Before exploring more deeply the nature of the "Li_2NiP_2" electrode and its Li-reactivity, it is interesting to evaluate the reversibility of this new D/E process. The capacity retention of the NiP_2/Li cell has been measured on the different potential windows [0, 2.0V], [0.25, 2.5V], [0.31, 2.5V] and [0.44, 2.5V] at a *C*/10 rate. The plots are reported Figure 2. Whereas the capacity retention rapidly fades on the [0, 2.0V] potential window, it is greatly improved on the [0.25, 2.5V], [0.31, 2.5V] and [0.44, 2.5V] ones. Thus, 95% of the 545 mA h g^{-1} initial reversible capacity is maintained after 12 cycles on the [0.25, 2.5V] potential window. It can be noticed that the first cycle capacity loss decreases when the potential window is restricted to the initial $NiP_2 \rightarrow$ "Li_2NiP_2" transformation. This demonstrates that the mechanism that takes place on charge from the Ni°/Li_3P electrode is less efficient than the one occurring from "Li_2NiP_2".

3.2. In situ XRD. In situ XRD measurements were performed in cycling the NiP_2/Li half-cell in the [0.31, 2.5V] potential window. Let us recall here that the discharge electrode at 0.31V is supposed to correspond to the intermediate "Li_2NiP_2". At first sight, the modifications observed in the XRD patterns upon charge seem to be limited to the vanishing of the "Li_2NiP_2" Bragg peaks at $2\theta = 21$ and 42.6° (illustrated by arrows on Figure 3). A deeper observation (see Figure 3a) emphasizes that both peaks shift toward higher angles during the removal of 0.5Li (i.e., during process S), and then continuously decrease in intensity up to the end of charge (i.e., during process D). This would suggest a single-phase process for S and a two-phase process for D. Surprisingly, the other Bragg peaks at 31.6 and 35.4° behave very differently. They are unchanged all along process S, start to broaden at the very beginning of process D, and are finally sharper and slightly shifted to higher angles at the end of process D (see Figure 3b). From a crystallographic point of view, this is consistent with the assumption that S and D are single- and two-phase processes, respectively, only if (i) the two pairs of peaks correspond to different (hkl) reflection planes with only one of them being affected by the structural modification occurring during process S, and (ii) the two phases involved in process D exhibit very close but different unit cell parameters regarding the other (*hkl*) planes. Note, however, that despite a significant peak broadening arising from the electrochemical grinding, a similar behavior is observed upon discharge (and subsequent cycles) for the two pairs of Bragg peaks, showing that S and D are perfectly reversible processes (Figure 4). From these results, it is clear that S corresponds to a narrow single-phase process from Li_2NiP_2 to $Li_{2-x}NiP_2$.

3.3. ^{31}P NMR Study. To complete the electrochemical and XRD characterizations, ^{31}P NMR experiments were undertaken on the full [0, 2 V] and the restricted [0.25, 2.5 V] potential windows. Note that due to complex signals arising from surface layers interfering with those of the active materials, we chose not to discuss the ^{7}Li NMR characterization in this paper. This technique is a power tool to survey the local environment of P atoms in lithiated phosphides. Only few ^{31}P MAS NMR characterization reports on TM phosphides exist in the literature, namely, Ni_3P[21] and Cu_3P, as well as Ni_2P and $Ni_{12}P_5$.[22] Moreover, TM phosphides may exhibit very different electronic structures and properties that are expected to lead to very different ^{31}P NMR characteristics, including absence of signal or impossibility to carry out such characterization. Facing the need to establish a correlation between the NMR characteristics and the electronic structures, we recently characterized a selection of binary lithium and V, Fe, Co, and Ni phosphides, using ^{31}P MAS NMR, and calculated their electronic structures.[23] Among them, we focused on the NiP_2 monoclinic phase. Its structure consists of corner-shared NiP_4 square-planes forming slightly warped layers. We clearly showed that the single P atom in the unit cell resonates at +185 ppm; the very long relaxation time of this signal as well as its temperature-independent NMR shift lying within the usual chemical shift range of P are characteristic of a diamagnetic compound, as was clearly shown by the electronic structure calculation.[23] Note that a small unidentified impurity peak was observed around −460 ppm in the starting NiP_2 sample (Figure 6, V0).

Prior to the study of the various charged/discharged electrodes, BM-Li_3P was studied by NMR. Li_3P has a hexagonal layered structure, S.G. *P6/mmm* (191), $a = 4.394$ Å and $c =$

(15) Bernardi, J.; Lemoigno, F.; Doublet, M.-L. *Ionics* **2008**, *14*, 197.
(16) Anisimov, V. I.; Zaanen, J.; Andersen, O. K. *Phys. Rev.* **1991**, *B 44*, 943.
(17) Anisimov, V. I.; Aryasestiawan, V.; Liechtenstein, A. I. *J. Phys.: Condens. Matter* **1997**, *9*, 767.
(18) Rundqvist, S. *Acta Chem. Scand.* **1961**, *15*, 451.
(19) Morcrette, M.; Gillot, F.; Monconduit, L.; Tarascon, J. M. *Electrochem. Solid-State Lett.* **2003**, *6*, 4.
(20) Delacourt, C.; Laffont, L.; Bouchet, R.; Wurm, C.; Leriche, J.-B.; Morcrette, M.; Tarascon, J.-M.; Masquelier, C. *J. Electrochem. Soc.* **2005**, *152* (5), A913.
(21) Furo, I.; Bakonyi, I.; Tompa, K.; Zsoldos, E.; Heinmaa, I.; Alla, M.; Lippmaa, E. *J. Phys.: Condens. Matter* **1990**, *18*, 4217.

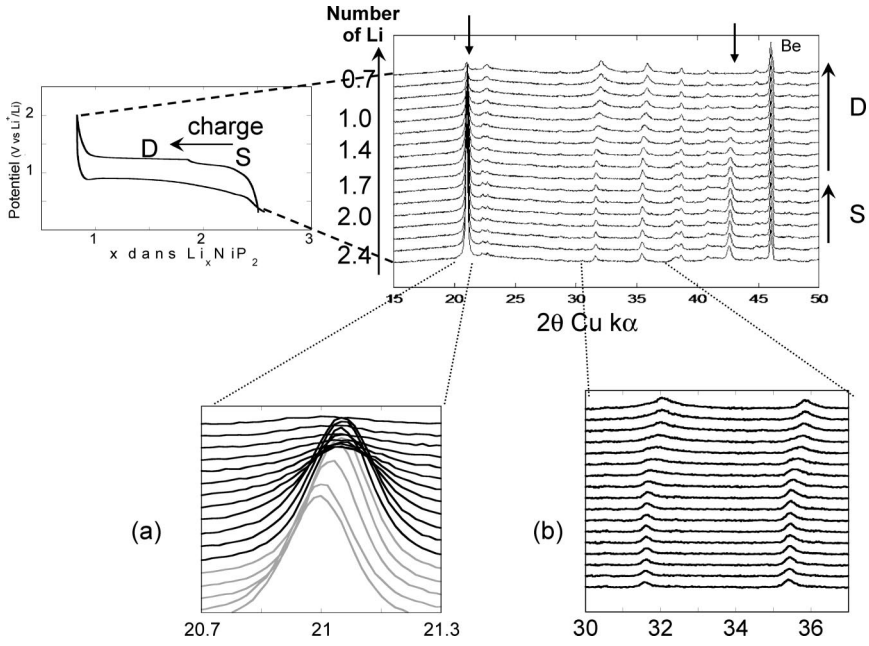

Figure 3. In situ X-ray diffraction patterns collected at various steps of charge for the NiP_2/Li electrochemical cell cycled in the restricted [0.31, 2.5 V] potential window. The stars stand for the Bragg peaks corresponding to the "Li_2NiP_2" electrode, whereas the beryllium characteristic peaks are indicated by Be.

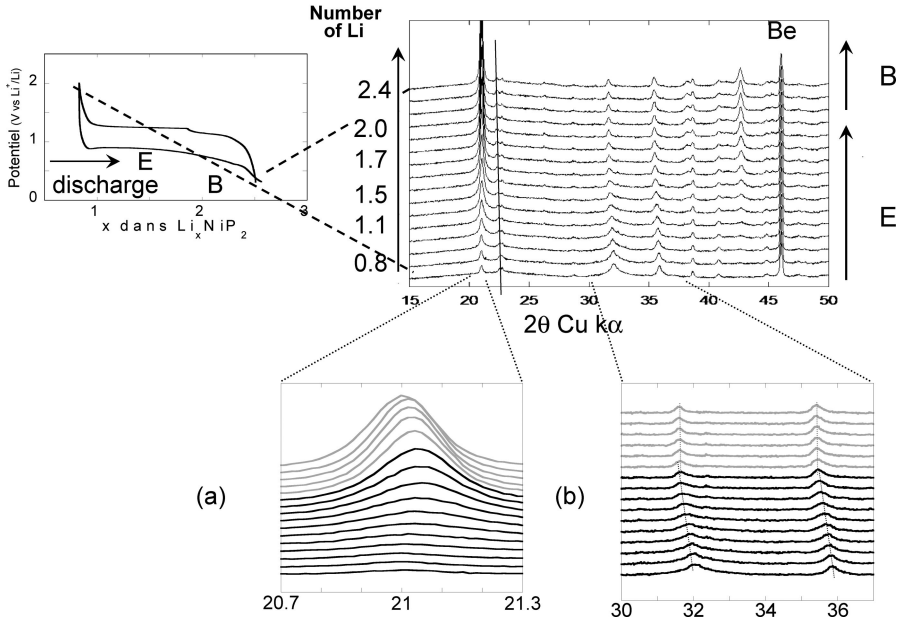

Figure 4. In situ X-ray diffraction patterns collected at various steps of discharge for the NiP_2/Li electrochemical cell cycled in the restricted [2.5, 0.31 V] potential window. As for Figure 3, the "Li_2NiP_2" and beryllium characteristic peaks are indicated by stars and Be, respectively.

7.581 Å, consisting in alternative Li and Li_2P layers. In this structure, P atoms occupy only one position 1a (0, 0, 0). The ^{31}P MAS NMR spectrum shown in Figure 5 is characterized by a major signal at ca. −278 ppm, in good agreement with the results reported by Tirado et al.[24] Note that impurity signals are observed in the 0 to 100 ppm range, as well as a broad shoulder at the bottom of the Li_3P signal. They must correspond to structurally disordered compounds as can be expected from the preparation method used.

The ^{31}P MAS NMR spectra were then recorded on "Li_xNiP_2" electrodes, at different stages of lithiation/delithiation within the [0, 2 V] and the [0.25, 2.5 V] potential windows, as reported in Figures 6 and 7.

On the [0, 2 V] Potential Window. As discussed above on the basis of XRD, the V1 phase corresponds to the "Li_2NiP_2" electrode. The ^{31}P MAS NMR signal clearly reveals traces of unreacted NiP_2. Due to its very long relaxation time, the amount of NiP_2 is somewhat underestimated in this experiment. A rather complex signal is also observed, with its decomposition into individual components shown in the inset of Figure 6. This yields a set of Gaussian-type components ranging from 100 to 200 ppm, with rather different residual linewidths, suggesting different types of P atoms, each with a distribution around a given characteristics. The experimental signals clearly show that the compound formed in the cell contains some disorder. In addition, the relaxation time for this electrode is short ($5T1 <$

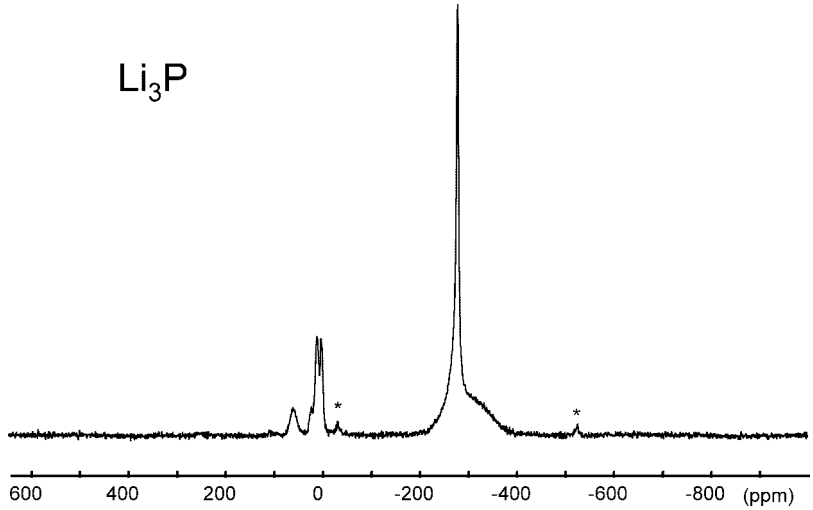

Figure 5. ^{31}P MAS NMR spectrum of Li_3P prepared by ball-milling in which stars stand for the spinning side bands.

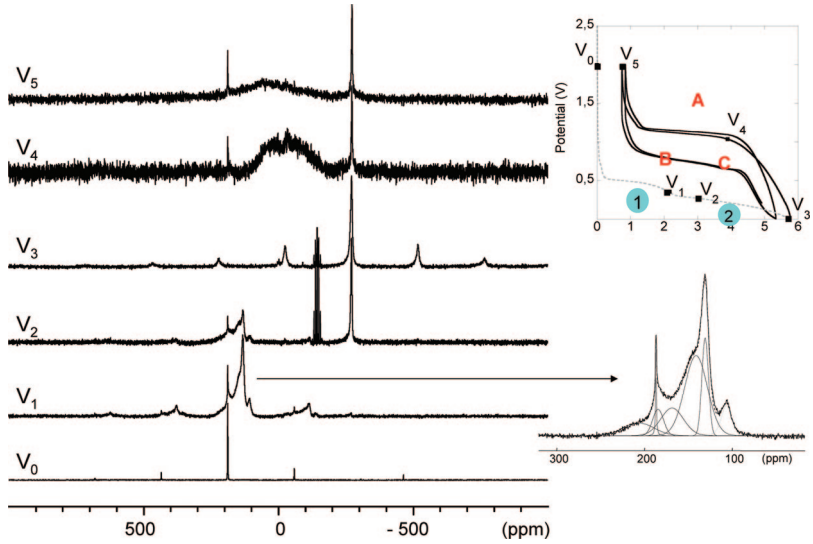

Figure 6. ^{31}P MAS NMR spectra of samples collected at various steps of discharge (V0, V1, V2, V3) and charge (V4, V5) fo the NiP_2/Li electrochemical cell cycled in the [0, 2 V] potential window. The associated galvanostatic curve is reminded together with the main electrochemical processes involved.

20 s), i.e., in the same order of magnitude as that of the metallic VP_2 system.[25]

Upon discharge to $x = 3$ (V2), the same NMR pattern is observed, including the remaining NiP_2, probably resulting from electrochemically disconnected grains in the electrode, together with the appearance of the Li_3P signal. This confirms that the conversion reaction from the "Li_2NiP_2" phase to Li_3P and metallic Ni is partial for this composition. A characteristic J-coupled multiplet is also observed, because of traces of PF_6^- salt from the electrolyte (see Experimental Section). The magnitude of this signal in the various samples is very sensitive to the washing procedure and the nature of the sample.

Upon discharge down to 0 V (V3), the signal of "Li_2NiP_2" has disappeared, and the only observable ^{31}P NMR signal is that of Li_3P showing the complete conversion. One can notice that the signal for Li_3P exhibits more spinning sidebands than that of the "model" ball-milled Li_3P (Figure 5). This is probably due to dipolar interactions from the neighboring superparamagnetic Ni particles (a 0.66 Am^2/Kg_{Ni} magnetization was measured for 5T at room temperature). Note that the V2 spectrum described above and corresponding to the initial appearance of Li_3P and metallic Ni° is comparatively not broadened despite the simultaneous formation of Li_3P and Ni°. This may be due to the effect of the remaining unconverted "Li_2NiP_2", and to the fact that the newly formed Ni° is not yet in the form of clearly superparamagnetic nanoparticles.

Upon further charge to 1.15 V (V4), Li_3P can still be observed together with a trace of starting NiP_2 and a very broad signal. Upon full charge to 2.0V (V5), a similar spectrum is observed again with some remaining traces of Li_3P and starting NiP_2 with a broad signal slightly different from the one after partial charge discussed above. It is

(22) Stinner, C.; Tang, Z.; Haouas, M.; Weber, Th.; Prins, R. *J. Catal.* **2002**, *208*, 456.
(23) Bekaert, E.; Bernardi, J.; Boyanov, S.; Monconduit, L.; Doublet, M.-L.; Ménétrier, M. *J. Phys. Chem. C*, published online Dec 3, http://dx.doi.org/10.1021/jp808122q.
(24) Bernardo, L.; Corredor, J. I.; Tirado, J. L.; Pérez-Vicente, C. *J. Electrochem. Soc.* **2006**, *153* (10), A1829–A1834.
(25) Gillot, F.; Ménétrier, M.; Bekaert, E.; Dupont, L.; Morcrette, M.; Monconduit, L.; Tarascon, J. M. *J. Power Sources* **2007**, *172* (2), 877.

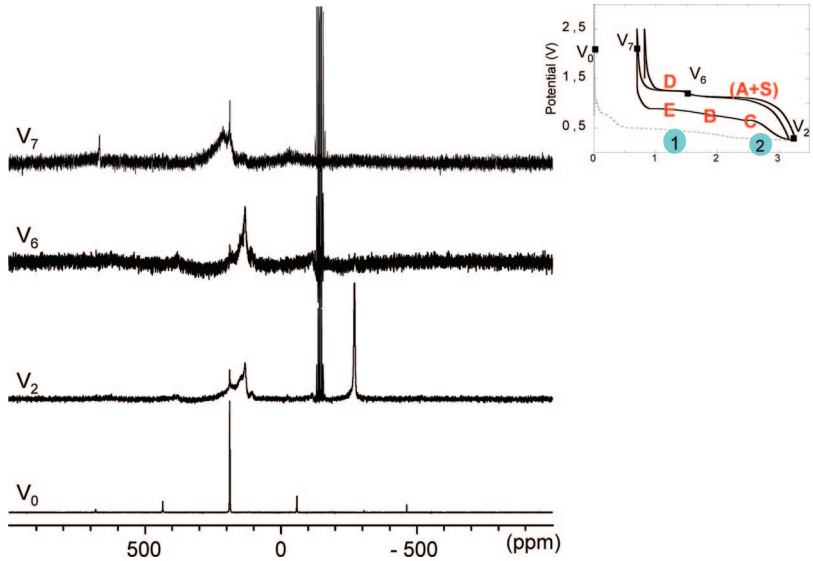

Figure 7. ^{31}P MAS NMR spectra of samples collected at various steps of discharge (V0, V2) and charge (V6, V7) for the NiP_2/Li electrochemical cell cycled in the [0.25, 2.5 V] potential window. The associated galvanostatic curve is reminded together with the main electrochemical processes involved.

therefore clear from this observation that Li_3P has not completely disappeared (note, however, that its line shape is no longer affected by the broadening assigned to Ni superparamagnetic particles), and also that the compound formed is very different from the starting NiP_2. Its signal suggests a considerable disorder (from the width of the line), and diamagnetic type properties (from the average NMR shift lying in the chemical shift range of P).

On the [0.25, 2.5 V] Potential Window. Note that the V0 and V2 spectra are recalled in Figure 7 for ease of comparison. Upon recharge from V2 to V6, the ^{31}P NMR signal shows that "Li_2NiP_2" is still present while the signal for Li_3P is no longer observed. This suggests that the Ni°/Li_3P part of the V2 composite electrode has already undergone a reconstruction process at V6, even though it is difficult to ascertain whether a broad component observed for V4 is present or not in the spectrum (probably hidden below the "Li_2NiP_2" signal). At this voltage (V6) the single phase process S is expected to be completed, showing that "Li_2NiP_2" and "$Li_{2-x}NiP_2$" exhibit similar ^{31}P NMR response.

Upon recharge from V6 to V7, a different type of spectrum is observed. It is significantly different from that of the V5 point, which suggests that a new "$Li_\varepsilon NiP_2$" is formed when charging "$Li_{2-x}NiP_2$" which is different from the one obtained when charging the converted Ni°/Li_3P (V5). This corroborates the electrochemical results showing that upon charge three distinct processes occur on the [0.25, 2.5 V] potential window (namely S, A, and D), whereas only two processes occurs on the [0, 2 V] potential window (namely S and A).

3.4. Phase Stability Diagram and Structural Characterization. First-principles DFT calculations were investigated to establish the $T = 0$ K Li−Ni−P_2 phase stability diagram and to characterize any of the possible intermediate ternary phases stabilized upon lithium insertion. The results presented in Figure 8 show that a few intermediate Li_xNiP_2 phases lie lower in energy than the converted Ni°/Li_3P in the composition range $x = 1.5 - 2.0$. Below and above this composition range, some metastable phases exist that could

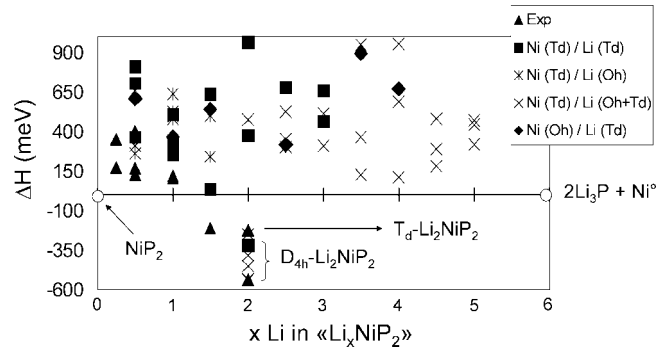

Figure 8. Li_x−Ni−P_2 phase stability diagram computed within the DFT formalism using the GGA-PBE functional. The formation energy of each model structure is plotted with respect to the reference energy of the conversion reaction (horizontal line). The labels refer to the five structural models used in the calculations, as input structures (prior to the structural relaxation).

be considered to be potentially obtainable under certain kinetic conditions. It should be recalled here that the structural types listed on Figure 8 stand for the input structures of the calculation, i.e., prior to the structural relaxations, and not to the fully relaxed ones. But, if we focus on the most stable phases, i.e. the fully relaxed phases lying below or a few k_BT (25 meV) above the reference enthalpy of the conversion reaction, only two structural types (among the five input ones) are found. Both of them correspond to layered structures in which NiP_2 and Li layers alternate along their normal axis (interlayer direction). In these structures, the short interlayer P−P contact occurring in the NiP_2 starting structure at 2.21 Å are broken, leading to a doubled interlayer distance favorable for Li insertion. The NiP_2 layers consist in corner-shared distorted NiP_4 tetrahedra (denoted T_d-Li_2NiP_2 in Figure 8) or in corner-shared NiP_4 square-planes (denoted D_{4h}-Li_2NiP_2 in Figure 8). In each structural type, namely, T_d or D_{4h}, the different structures obtained differ from one another by (i) the lithium distribution over the different sites occurring in the Li layers and/or (ii) the warping of the NiP_2 layers and/or (iii) the shift between two successive NiP_2 layers. Interestingly, all the T_d-Li_2NiP_2

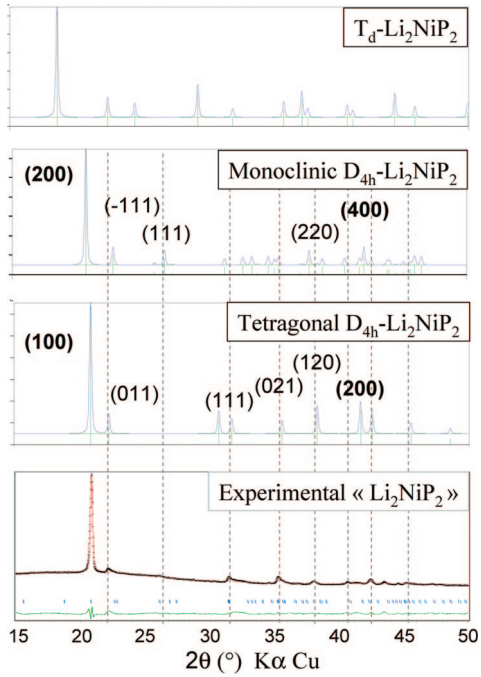

Figure 9. X-ray diffraction patterns simulated for the T_d-Li_2NiP_2, the monoclinic D_{4h}-Li_2NiP_2 and the tetragonal D_{4h}-Li_2NiP_2 phases as obtained from first-principles calculations compared to the (experimental) in situ XRD patterns collected on the "Li_2NiP_2" electrode, as obtained from cycling the NiP_2/Li cell in the restricted [0.31, 2.5 V] potential window.

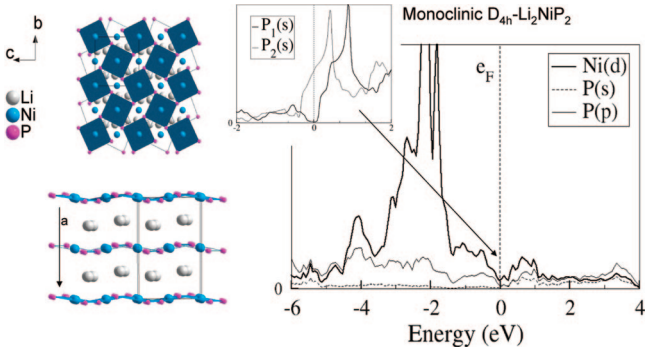

Figure 10. Crystal structure (left) and partial density of states (projected on the Ni(d), P(s), and P(p) atomic levels) of the monoclinic D_{4h}-Li_2NiP_2 as computed from first-principles DFT calculations.

structures are systematically less stable than the D_{4h}-Li_2NiP_2 ones by at least 250 meV (10 k_BT), independently of criteria i−ii−iii. Moreover, their constitutive NiP_4 tetrahedra are significantly flattened along the interlayer axis. These two latter observations strongly suggest that the T_d-Li_2NiP_2 structures are local minima in the potential energy surface of Li_2NiP_2 and that the D_{4h}-Li_2NiP_2 structural type is the most probable one to be electrochemically obtained upon charge and discharge. As a confirmation, we compared the X-ray diffraction patterns collected on the "Li_xNiP_2" electrodes ($2.0 \leq x \leq 2.4$) to the ones simulated for the different T_d-type structures. As shown Figure 9 for the most stable T_d-like phase, there is no agreement between the two XRD patterns. From now on, we will therefore focus on the different D_{4h}-Li_2NiP_2 phases highlighted by our phase diagram. As shown in Figures 10 and 11, the most stable D_{4h}-Li_2NiP_2 phases differ from the warping and the shift of their NiP_2 layers of corner-sharing square-planes. They

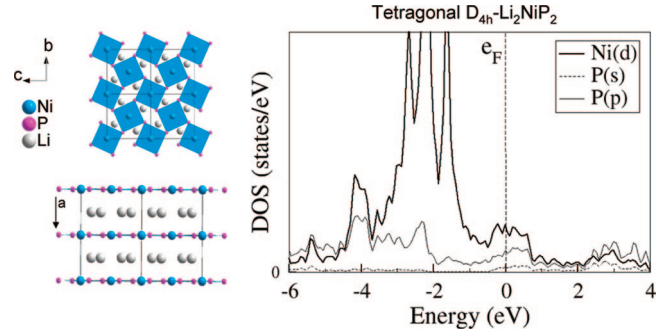

Figure 11. Crystal structure (left) and partial density of states (projected on the Ni(d), P(s), and P(p) atomic levels) of the tetragonal D_{4h}-Li_2NiP_2 as computed from first-principles DFT calculations.

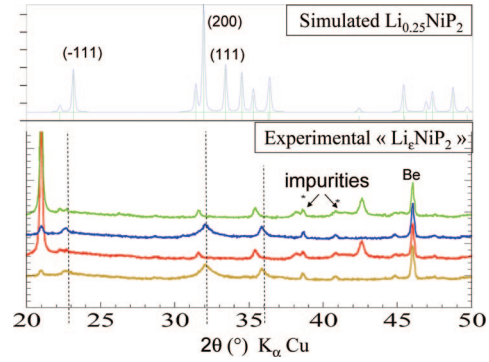

Figure 12. X-ray diffraction patterns simulated for the $Li_\varepsilon NiP_2$ phase as obtained from first-principles calculations, compared to the (experimental) in situ XRD patterns collected on the fully charged electrode in the [0.31, 2.5 V] potential window.

crystallize either in a monoclinic space group ($P2_1/c$) with unit cell parameters $a = b = 5.68(1)$ Å, $c = 8.96(1)$ Å and $\beta = 106.6°$ when the NiP_2 layers are slightly warped and shifted from one to another (see Figure 10), or in a tetragonal space group *(P4/mbm)* with unit-cell parameters $a = b = 5.64(1)$ Å and $c = 4.25(1)$ Å when they are perfectly superimposed and planar (see Figure 11). Due to the doubled unit cell of the monoclinic structure compared to the tetragonal one, there are two different P atoms in the former and one only in the latter. Note that this shift bears some similarity with the phase transition occurring between the graphene planes when lithium is inserted into the graphite electrode.[26] Interestingly, the energy difference between these two phases is less than 10 meV per formula unit, i.e., they may be considered as iso-energetic. Moreover, the nickel ions show exactly the same environment in the D_{4h}-Li_2NiP_2 phases than in the starting NiP_2. This suggests similar Ni^{+II} oxidation states in these phases, as confirmed by the partial density of states of NiP_2 and D_{4h}-Li_2NiP_2.[15] The main structural modification under concern is the breaking of the short interlayer P−P bonds of the NiP_2 starting structure. This clearly demonstrates that P is the main redox center of the reduction from NiP_2.

The XRD patterns simulated for the monoclinic and the tetragonal phases are presented in Figure 9 as a comparison to the experimental XRD patterns recorded on the electrode

(26) Hérold, A.; In *Chemical Physics of Intercalation*; Legrand, A. P., Flandrois, S., Eds.; NATO ASI Series, Series B, Physics; Springer: New York, 1987; Vol. 172, p 3.

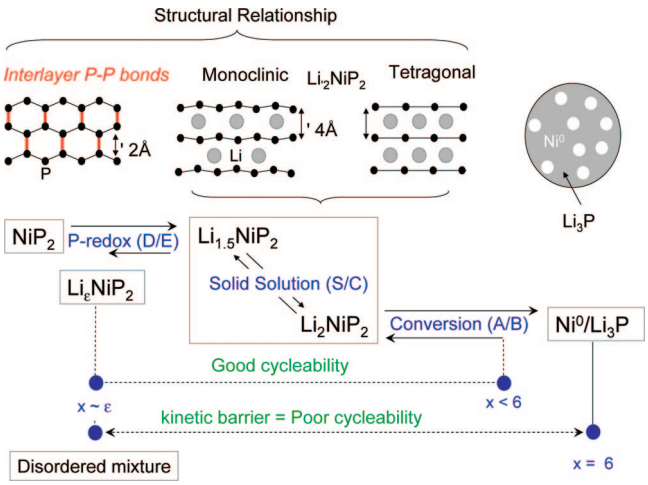

Figure 13. Full redox mechanism for the lithiation of the NiP_2 electrode. The crystal structures of the Li_xNiP_2 ($x = 0.25$, 1.5, 2.0) are illustrated by more or less warped and/or shifted NiP_2 layers (black) with Li (gray circles) in between. The electrochemical reactions are represented by horizontal (two-phase process) or sloppy (single-phase process) lines, respectively. For each process, the composition range for which the reversibility is optimum is indicated by dotted lines.

obtained at 0.31 V on first discharge ("Li_2NiP_2"). Both structures show (*h*00) reflections around 21 and 42°, characteristic of the interlayer distance (*a*-axis), in perfect agreement with the similar behavior observed experimentally for these two peaks upon charge and discharge (see section 3.2). All other reflections are quite different for the two structures, because of their different features regarding the warping and the shift of their NiP_2 layers, in good agreement with our previous assumption that the two pairs of Bragg peaks at 21°/42.6° and 31.6°/35.4° should correspond to different (hkl) reflections. A pretty good agreement is observed between the XRD patterns of the tetragonal phase and those of the experimental "Li_2NiP_2" electrode. It should be noticed however that the very small peak observed around 26.8° in the experimental XRD patterns does not correspond to any reflection of the tetragonal structure. It could correspond to the (111) Bragg peak of the monoclinic structure, which finds some consistency with the electrochemical and ^{31}P NMR results. Indeed, the fact that the ^{31}P NMR signal of V1 (supposed to be majoritary "Li_2NiP_2") can be decomposed into many different signals supports the occurrence of the monoclinic phase in the electrode (even in a small amount) and therefore the response of more than one P atoms.

It is now interesting to correlate the ^{31}P NMR response of the "Li_2NiP_2" electrode to the general feature of the electronic structures of the monoclinic and tetragonal single phases. To that aim, we computed their electronic band structure and density of states. Since Ni−Ni magnetic interactions could occur in these structures, spin-polarized calculations were performed using ferromagnetic and antiferromagnetic spin configurations as inputs, prior to the structural relaxations. The DFT+U formalism was also applied to check the stability of the results over the correlation parameter U_{eff} ranging from 0 to 4 eV. These values are chosen with respect to those reported in the literature for nickel oxides,[27] assuming that the self-interaction error in (more covalent) transition metal phosphides is expected to be minimized compared to transition metal oxides. The results are presented in Figures 10 and 11 in the DFT limit ($U = 0$ eV) for the monoclinic and the tetragonal phases, respectively. For the two structures, no spin-polarization occurs whatever the U_{eff} parameter and the magnetic structure considered in the calculations, i.e., ferromagnetic or antiferromagnetic. The monoclinic phase shows a semimetallic behavior in the DFT limit ($U = 0$ eV) which turns to a small gap semiconductor as U_{eff} is increased up to 4 eV (see the Supporting Information). According to our previous work on NiP_2[23] a value of $U_{eff} \approx 2$ eV is likely to be the right parameter for the nickel diphosphide NiP_2. The two P atoms occurring in the monoclinic unit cell show different P(s) contributions at the Fermi level in the semimetallic state as shown in the inset of Figure 10 for $U = 0$ eV which is consistent with the occurrence of different ^{31}P NMR signals for "Li_2NiP_2". The tetragonal phase shows a metallic behavior, independently of the U_{eff} value considered. This is in very good agreement with the short relaxation time measured for the "Li_2NiP_2" (V1) electrode (characteristic of a metallic behavior) and with the reasonable match of the experimental and simulated XRD patterns. The tetragonal phase thus appears to be primarily the one electrochemically obtained upon cycling, although the occurrence of a small amount of the monoclinic D_{4h}-Li_2NiP_2 (lying only a few meV above the tetragonal phase in our phase stability diagram) cannot be completely ruled out. The different NMR signals observed for the P atoms in the V1 electrode may thus be associated to a disorder arising from phosphorus in surface and/or from a reminiscent warping and shift of the NiP_2 layers, as it occurs in the starting NiP_2 and in the monoclinic D_{4h}-Li_2NiP_2.

The remaining question to be addressed is the nature of the fully charged "$Li_\epsilon NiP_2$" electrode. When directly charged from the Ni°/Li_3P composite (V5), this electrode looks like a strongly disordered phase mixed with traces of unreacted products. The broad NMR signal and the absence of XRD peaks support this hypothesis that complete oxidation from Ni°/Li_3P does not occur at the thermodynamic equilibrium. When charged from the "Li_2NiP_2" electrode, the "$Li_\epsilon NiP_2$" (V7) electrode shows an NMR signal different from V5 and from the starting NiP_2 (V0) and has been shown to result from two reversible processes assigned to a solid solution from "Li_2NiP_2" (process S) and a two-phase reaction from "$Li_{(2-x)}NiP_2$" (process D). From our phase stability diagram, only one phase of composition $Li_{1.5}NiP_2$ lies lower in energy than the conversion reaction. Its crystal structure is very close to the tetragonal Li_2NiP_2 regarding the planar shape of the NiP_2 layers, and very close to the monoclinic Li_2NiP_2 regarding their shift. Interestingly, the XRD patterns of this $Li_{1.5}NiP_2$ phase are very close to those simulated for the monoclinic Li_2NiP_2, which is consistent with the disorder deduced from the complex ^{31}P NMR signal and with the single-phase process observed in oxidation from the "Li_2NiP_2" electrode. This also suggests a (energetically) free

(27) Zhou, F.; Cococcioni, M.; Marianetti, C. A.; Morgan, D.; Ceder, G. *Phys. Rev. B* **2004**, *70*, 235121.

motion of the NiP_2 layers with respect to one another in this composition range and therefore the probable occurrence of a turbostratic disorder in the electrode during the single-phase process. Below $x = 1.5$, some metastable Li_xNiP_2 phases are found, a few tens of k_BT above the conversion reaction. Although these phases might be stabilized by entropy effects associated with disordered Li distributions, it is unlikely that they could gain enough energy to reach the conversion line, because the configuration entropy term generally contributes to the total energy by a few millielectronvolts at room temperature ($T = 300$K). It is worth noting, however, that all stable Li_xNiP_2 structures ($x \leq 1$) are described by NiP_2 layers which are all the more warped as the Li content decreases. At $x = 0.25$, the structure of NiP_2 is nearly recovered and the simulated XRD patterns are comparable to those of the NiP_2 starting material. As shown Figure 12, the main (h00) Bragg peaks at 21 and 42.6° of the experimental "Li_2NiP_2" electrode have disappeared in the "$Li_\varepsilon NiP_2$" XRD patterns, exactly as in the simulated XRD patterns of $Li_{0.25}NiP_2$. A good agreement is also found for the Bragg peak around 32°, which corresponds to the main reflection peak of the $Li_{0.25}NiP_2$ phase, characteristic of the interlayer (200) plane. Provided that the two peaks around 38.5 and 41° are associated with impurities, the other Bragg peaks of the $Li_{0.25}NiP_2$ phase could match the experimental XRD patterns of the "$Li_\varepsilon NiP_2$" electrode, in a quite reasonable agreement.

4. Discussion

Combining electrochemical, XRD and ^{31}P NMR experimental characterisations with first-principles calculations now allows us to fully interpret the redox mechanism of the NiP_2 negative electrode, including (i) the Li-reactivity of the discharged Ni°/Li_3P composite and the Li_2NiP_2 intermediate phase, and (ii) the structural characterization of all the intermediate phases obtained upon charge and discharge. As already shown in our previous report,[10] NiP_2 reacts with 6Li through a two-step electrochemical process whereby an intermediate "Li_2NiP_2" electrode is first formed and then converts into the nanocomposite Ni°/Li_3P electrode, following the general chemical equations

$$NiP_2 + 2Li \rightarrow Li_2NiP_2 \text{ (insertion)}$$

$$Li_2NiP_2 + 4Li \rightarrow Ni° + 2Li_3P \text{ (conversion)}$$

The experimental and theoretical investigations reported in the present work lead to consistent results as concern the intermediate "Li_2NiP_2" electrode. It is a ternary Li_2NiP_2 single phase that crystallizes in the *P*4/*mbm* tetragonal space group with unit-cell parameters $a = b = 5.64(1)$ and $c = 4.25(1)$ Å. This computed crystal structure is consistent not only with our previous SAED analysis[10] (for the tetragonal symmetry and the unit cell parameters) but also with the XRD patterns of the "Li_2NiP_2" electrode. Its electronic structure correlates well with the ^{31}P NMR signal and the relaxation time of the corresponding "Li_2NiP_2" electrode (V1), although our calculations cannot reproduce the considerable disorder experimentally observed for the phosphorus atoms.

Interestingly, whether this ternary Li_2NiP_2 phase occurs or not in the electrode plays a key-role on the redox mechanism of the starting NiP_2 and correlatively on the cycleability of the associated cell. Its Li-reactivity has been clearly interpreted as the result of two distinct processes in oxidation and only one process in reduction. The oxidation of Li_2NiP_2 first follows a narrow single-phase process associated with the removal of ~0.5 Li, and then transforms into the $Li_\epsilon NiP_2$ phase, through a two-phase process. From our calculations, the latter is proposed to be structurally very close to the starting NiP_2, with probably a very small amount of Li trapped in the interlayer spacing.

Regarding the cycleability of Li_2NiP_2, the two distinct electrochemical processes emphasized in the present work are shown to be perfectly reversible in the restricted [0.31, 2.5 V] potential window, leading to very good capacity retentions (~95%) after 12 cycles (see Figure 2). Such a good reversibility is very likely to originate from the strong structural relationship between all the intermediate Li_xNiP_2 phases achieved in this potential window, i.e. between $x = 0$ and $x = 2.2$. In reduction, the Li_2NiP_2 phase undergoes a conversion reaction to form the nanocomposite Ni°/Li_3P electrode, as clearly demonstrated by the in situ XRD patterns and the ^{31}P NMR signal of the corresponding electrodes (V2 and V3 for the full [0, 2 V] potential window), as well as by the absence of any stable phase in our computed phase stability diagram in the $2 \leq x \leq 6$ composition range. Surprisingly, the reoxidation of the Ni°/Li_3P electrode does not allow for a reconstruction of the starting NiP_2. On one hand, an unidentified disordered phase (broad signal centered at 100 ppm) and unreacted traces of Li_3P and NiP_2 can be deduced from the ^{31}P NMR signals. On the other hand, the in situ XRD patterns (not shown here) show very broad and weakly intense peaks indicative of an amorphous and/or nanosized electrode, with no evidence for Li_2NiP_2 phase. The occurrence of unreacted phases shows that the oxidation process from Ni°/Li_3P is kinetically limited, and naturally leads to a rather poor cell cycleability in the full [0, 2 V] potential window (see Figure 2). Further experiments at thermodynamic equilibrium, using galvanostatic intermittent titration technique (GITT), are currently in progress to get more insights into the thermodynamic/kinetic competitions in such transition metal phosphides and to check whether mixed electrodes involving Li_xNiP phases with unreacted Li_3P could be formed upon oxidation. Note that in addition to these kinetic limitations, parasitic reactions with the electrolyte could also be responsible for the poor cycleability of the cell. These reactions generally occur at very low potential and could be promoted by the nanosized character of the fully discharge Ni°/Li_3P composite. These results confirm that oxidation process from Ni°/Li_3P can no longer be associated with the same electrochemical reaction than the one taking place from the electrode discharged in the restricted [0.31, 2.5 V] potential windows. The oxidation process from the composite Ni°/Li_3P electrode corresponds to a kinetically limited transformation into an unidentified disordered mixture, different from the starting NiP_2.

The key-point of the study arises from the electrochemical test performed on the [0.25, 2.5 V] restricted potential

window, i.e. when the starting NiP_2 is discharged down to $x = 3.6$ prior to be recharged. As discussed above, the first part of the first discharge corresponds to the formation of the intermediate Li_2NiP_2 phase. Going further along the reduction process (i.e., from $x = 2$ to $x = 3.6$) leads to the partial conversion of Li_2NiP_2 into the nanocomposite Ni°/Li_3P electrode. At 0.25V, the electrode thus consists in a proportional mixture of Li_2NiP_2 and Ni°/Li_3P. Interestingly, this cell shows a much better cycleability than the one cycled within the full [0, 2V] potential window. Moreover, all the processes identified for the redox mechanism of Li_2NiP_2 are fully recovered in this [0.25, 2.5V] potential window, including the reconstruction of the $Li_\epsilon NiP_2$ in charge. This demonstrates that the conversion reaction is reversible as long as the discharged electrode contains traces of Li_2NiP_2. In other words, the kinetic limitation of the reaction which transforms the composite Ni°/Li_3P electrode into a disordered charged electrode appears to be linked to a nucleation delay of Li_2NiP_2. As a consequence, the best compromise between cycleability and capacity should be reached for potential windows allowing the highest faradic balance (as close to $x = 6$ as possible) but preventing the complete conversion of Li_2NiP_2 into Ni°/Li_3P. This is fully confirmed by the similar cell cycleability obtained in the restricted potential windows (see Figure 2), no matter the lower voltage limit for the end of discharge (provided that it is greater than 0), i.e., independently of the amount of Li_2NiP_2 occurring in the discharged electrode. Hence, Li_2NiP_2 is required in the electrode, even in small amounts, to favor the reversibility of the conversion reaction, and then to improve the cycleability of the NiP_2/Li cell.

The redox mechanism of NiP_2 is now fully rationalized, as summarized in the qualitative picture of Figure 13. Compared to our previous studies, a new electrochemical mechanism has been clearly elucidated and all intermediate electrodes have been fully characterized. The Li-reactivity of NiP_2 is now decomposed in three successive reactions clearly identified as a biphasic insertion, a monophasic insertion (solid solution) and a conversion reaction in the ($0.0 \leq x \leq 1.5$), ($1.5 \leq x \leq 2.0$), and ($2.0 \leq x \leq 6.0$), respectively. The former two are perfectly reversible, probably because of the strong structural relationship that exists between all phases involved in these electrochemical reactions. By opposition, the latter process involves phases with no structural relationship and is kinetically limited. This kinetic limitation has been rationalized in terms of a nucleation delay of the Li_2NiP_2 phase, thus providing alternative routes to improve the performances of the transition metal phosphides, as negative electrode for Li-ion battery.

5. Concluding Remarks

The study reported in this paper combines various experimental (electrochemical tests and in situ XRD and ^{31}P NMR characterizations) and computational techniques to fully rationalize the lithium reactivity of the NiP_2 electrode, and to improve the cell cycleability. As already reported for other transition metal phosphides such as FeP for instance,[6] NiP_2 requires a two-step insertion/conversion reaction to fully convert into the nanocomposite Ni°/Li_3P electrode. This is different from transition metal oxides for which the conversion reaction is generally direct. The explanation for such different behaviours lies in the nature of the M-P bonds which are much more covalent than the M−O ionic bonds, thus yielding very different electronic structures for these compounds around the Fermi level, i.e. for the electronic states involved in the redox activity of the compounds. The high-lying energy of the P(3s,3p) atomic levels compared to the O(2s,2p) gives rise to pure P-like electronic levels at the Fermi level, while mainly metallic levels occurs in this energy range for transition metal oxides. As a consequence, P is the main redox center for the first-step insertion reaction of NiP_2 as fully confirmed by the Ni local environment and formal oxidation state, which both remain constant all along the insertion reaction from NiP_2 to Li_2NiP_2. This first-step insertion is the result of two successive processes, and not one process only as previously reported: a biphasic process associated with the exchange of 1.5Li and resulting in the breaking of the interlayer P−P bonds of the starting NiP_2 and a monophasic process associated with the exchange of 0.5Li defining a narrow solid solution domain up to Li_2NiP_2. Interestingly, whereas the intermediate Li_2NiP_2 phase is easily obtained from an electrochemical route, it has not yet been synthesized through classical ceramic routes. Moreover, its occurrence in the electrode plays a key role in the cycleability of the NiP_2/Li cell in decreasing the kinetic limitation linked to its nucleation, therefore improving the reversibility of the conversion process.

Finally, despite the approximations used in our calculations (i.e., bulk calculations at $T = 0$ K) the method used to compute phase stability diagrams is a powerful tool for designing and characterizing the most probable phases potentially achieved upon charge/discharge, before the full conversion reaction. This method has been successfully applied to other transition metal phosphides, showing that if provides reasonable explorations of the Li_xMP_y potential energy surfaces, and that surface/interface interactions should not dominate the electrochemical reactivity of the studied electrodes, at least for the first cycles.

Acknowledgment. Authors thank M. Morcrette from the LRCS (University Amiens) for the in situ XRD measurements. This research was performed in the framework of ALISTORE Network of Excellence (Contract SES6-CT-2003-503532) founded by the EC. We would like to thank the ADEME (Agence de l'Environnement et de la Maîtrise de l'Energie) for its financial support through the PhD grants of S.B. and J.B.

Supporting Information Available: Additional figures (PDF). This material is available free of charge via the Internet at http://pubs.acs.org.

CM802393Z